VALIDATIONS AND APPLICATIONS OF THE FEAST CODE [1]

Z. Xu [2], M. Tayal [2], J.H. Lau [2], D. Evinou [2] and J.S. Jun [3]

ABSTRACT

The FEAST (Finite Element Analysis for Stresses) code is part of a suite of computer codes that are used to assess the structural integrity of CANDU® fuel elements and bundles. A detailed validation of the FEAST code was recently performed. The FEAST calculations are in good agreement with a variety of analytical solutions (18 cases) for stresses, strains and displacements. This consistency shows that the FEAST code correctly incorporates the fundamentals of stress analysis. Further, the calculations of the FEAST code match the variations in axial and hoop strain profiles, measured by strain gauges near the sheath-endcap weld during an out-reactor compression test. The code calculations are also consistent with photoelastic measurements in simulated endcaps.

INTRODUCTION

The FEAST code is part of a suite of computer codes that are used to assess the structural integrity of the CANDU fuel element and bundle. Specifically, the FEAST code is used to calculate the detailed work densities, stresses, strains and displacements at sheath-endcap junctions, at circumferential ridges, at sheath-bearing pad junctions, in endplates, and in plenums. Examples[1] of applications of the FEAST code include stress concentration at sheath-endcap welds, circumferential ridge of sheath, stress distribution in endplates resulting from gravitational loads of fuel elements, creep collapse of sheath onto pellets under coolant pressure, and thermal stresses in graphite plenums. An earlier version of the FEAST code is also embedded in the ELESTRES code[2], for calculation of hourglassing of UO_2 pellets.

The FEAST code models elastic, thermal, plastic and creep stresses, strains, and displacements in solids subjected to concentrated, distributed or gravitational loads. The finite-element method is used to solve the classical equations describing the above processes in two-dimensional non-linear systems. The versatility of the finite-element method enables the users to define arbitrary geometries to capture the detailed stress concentrations such as at sheath-endcap junctions. A major strength of the code is the use of specialized numeric schemes that provide accurate yet fast and stable solutions for the severely non-linear situations normally encountered in the assessment of CANDU fuel.

The FEAST code was previously tested against a number of analytical solutions[1]. To meet current software quality assurance (SQA) requirements, a detailed validation of the code (version 2.2) was performed using the validation-matrix approach, that included the following activities:

- creating validation matrices that include a scenario-to-phenomenon table that specifies phenomena expected to occur during scenarios, and a phenomenon-to-data-set table that associates the phenomena to data sets that can be used to validate the modelling of phenomena;
- regrouping data sets (cases) according to the features in the FEAST code; formulating the cases to test features; forming a feature-based test matrix that consists of 20 test cases based on the phenomena modelled, for example, the convergence test cases, cases involving elastic stress distributions, plastic stress distributions, creep situations etc; all features listed in the feature-based test matrix were tested;

---

[1] Presented at the 6th International Conference on CANDU Fuel, Canadian Nuclear Society, 1999 September 26-29.

[2] Atomic Energy of Canada Limited, Mississauga, Ontario, Canada.

[3] Korea Atomic Energy Research Institute.

- finding analytical solutions or experimental observations for all the test cases; and
- comparing the FEAST calculations with the analytical solutions or experimental observations for test cases.

The current paper describes the results of some typical cases from this study. As well, some illustrations of applications of the code are given.

VALIDATION MATRICES

As noted earlier, the FEAST code has been frequently used to assess the structural integrity of the CANDU fuel element and bundle. Six postulated scenarios regarding CANDU fuel were identified for application of the FEAST code (see Table 1). For each of these scenarios, a number of phenomena are expected to occur. These scenarios and their corresponding phenomena are listed in Table 1 (the scenario-to-phenomena table).

The phenomena were sorted and grouped based on their nature (see Table 2). A number of data sets were found to validate the modelling of a phenomenon; these are shown in Table 2. Table 2 is a phenomenon-to-data-set table that associates the phenomena to data sets that can be used. Tables 1 and 2 represent the validation matrices.

Data sets (cases) listed in Table 2 can be re-organized, according to the features of the FEAST code. Hence a feature-based test matrix (Table 3), consisting of 20 cases (data sets), was created. These cases cover modelling of elastic, thermal, plastic or creep stresses in a solid subjected to concentrated loads, distributed loads, thermal loads, multiple loads, cyclic loads or loading-unloading. They also account for material property changes such as yield strength variation caused by temperature change. These features were tested separately in separate cases. The FEAST code was also tested for convergence with mesh refinement and with time-step reduction.

There are 4 series of test cases: series 1, 2 and 3 consist of cases that can be solved analytically; series 1 contains the convergence test cases; series 2 includes the cases for elastic and thermal stress problems; series 3 consists of the cases for plastic and creep stress problems, and series 4 has the cases that can be compared with experimental observations.

Applications of the FEAST code will be illustrated after the validation cases are discussed. Although the overall results will be summarized in the current paper, only a few typical cases are discussed in detail because of space limitations. In the sections that follow, for each typical case a description will be given first, independent solutions (analytical or experimental) will then be discussed, and finally the calculations of the FEAST code will be compared with the independent solutions.

COMPARISONS WITH ANALYTICAL SOLUTIONS

Case 1-1 (mesh convergence test)

Consider a long thick-walled hollow cylinder whose inner surface is subjected to pressure p (Figure 1a). The radii of the inner and outer surfaces of the hollow cylinder are R_I and R_O. Find radial and hoop stress distributions along the radius in the wall.

(a) An analytical solution for this problem is available in the open literature[3]. The radial and hoop stresses are[3]

$$\sigma_r = \frac{R_i^2 p}{R_0^2 - R_i^2}(1 - \frac{R_0^2}{r^2}),$$

$$\sigma_\theta = \frac{R_i^2 p}{R_0^2 - R_i^2}(1 + \frac{R_0^2}{r^2})$$

The input parameters used were R_i = 51.7 mm, R_0 = 55.9 mm, and p = 10.9 MPa.

(b) FEAST calculations: hexagonal meshes, internally generated by the FEAST code, were used. The differences between analytical solutions and FEAST calculations based on the different meshes (different number of radial nodes) are illustrated in Figure 1b. It is seen that the differences decrease as the mesh becomes finer. This change shows that the FEAST code converges with mesh refinement. When a mesh with 10 radial nodes is used, the differences between the FEAST calculated and the analytically computed maximum radial stress and hoop stress are in the range of -0.12% to -0.02%.

Case 1-2 (time-step convergence test)

Consider a slab of length L and width W under uniaxial tension (see Figure 2). Assume that creep behaviour of the material obeys the Bailey-Norton law[4]: $\varepsilon_C = B\sigma^m t^n$, with $m = 2$ and $n = 1$. The initial loading stress is assumed σ_0. Find creep stress during stress relaxation in the slab.

(a) An analytical solution for this problem is available for m > 1[4]:

$$\sigma^{1-m} = \sigma_0^{1-m} + (m-1)\cdot E \cdot B \cdot t^n$$

The input parameters used were L = 40 mm, W = 20 mm, σ_0 = 200 MPa, m = 2, n = 1, E = 170 GPa, $B = A \cdot exp(-19300/1.986/T_0)$, T_0 = 273 K, and $A = 3.48\times10^{-6}$. The results of the analytical solution are shown in Figure 3a.

(b) FEAST calculations using different time steps: A mesh of 6 nodes in x direction and 11 nodes in y direction was used. The mesh represents one quarter of the area of the slab, as indicated in Figure 2. A displacement corresponding to the initial stress was applied. The FEAST predictions using different time steps are compared with analytical solutions in Figure 3a. It is seen that the FEAST calculations converge with time-step reduction (Figure 3b). When a time step of 0.01 h is used, the differences between the FEAST calculated and the analytically computed axial stresses at time of 6 h are within -0.1% (Figure 3b).

Case 2-8 (thermal stresses in a solid cylinder with parabolic temperature gradient)

Consider a long solid circular cylinder (Figure 4a) in which temperature changes parabolically along the radius (Figure 4b). If axial strain is constrained to be zero, find thermal stresses in radial, circumferential and axial directions.

(a) An analytical solution for calculations of thermal stresses and radial displacement in a solid cylinder is available in the open literature[5]:

$$\sigma_r = \frac{\alpha \cdot E}{1-\nu}(\frac{1}{R_0^2}\int_0^{R_0} Trdr - \frac{1}{r^2}\int_0^r Trdr),$$

$$\sigma_\theta = \frac{\alpha \cdot E}{1-\nu}(\frac{1}{R_0^2}\int_0^{R_0} Trdr + \frac{1}{r^2}\int_0^r Trdr - T),$$

$$\sigma_z = \frac{\alpha \cdot E}{1-\nu}\left(\frac{2}{R_0^2}\int_0^{R_0} Trdr - T\right),$$

$$\delta_r = \frac{(1+\nu)\alpha}{1-\nu}\left(\frac{1-3\nu}{1+\nu}\frac{r}{R_0^2}\int_0^{R_0} Trdr + \frac{1}{r^2}\int_0^{r} Trdr\right).$$

An analytical solution can be obtained by substituting temperature profile into the above equations and performing the integration. If the form $T = q + sr^2$ is used, the thermal stresses in radial, hoop and axial directions can be obtained as follows:

$$\sigma_r = \frac{\alpha \cdot E \cdot s}{4(1-\nu)}(R_0^2 - r^2),$$

$$\sigma_\theta = \frac{\alpha \cdot E \cdot s}{4(1-\nu)}(R_0^2 - 3r^2),$$

$$\sigma_z = \frac{\alpha \cdot E}{1-\nu}\left[2\nu\left(\frac{q}{2} + \frac{s}{4}R_0^2\right) - (q + sr^2)\right],$$

$$\delta_r = \frac{(1+\nu)\alpha}{1-\nu}\left[(1-2\nu)\left(\frac{q}{2} + \frac{s}{4}R_0^2\right) + \left(\frac{q}{2} + \frac{s}{4}r^2\right)\right]r.$$

The input parameters used in the analysis were $R_0 = 6$ mm, $E = 170$ GPa, $\alpha = 10^{-5}$ 1/K, $\nu = 0.3$, $s = -3.1952 \times 10^7$ K/m^2, and $q = 1488.6$ K. Analytical solutions of displacement and thermal stresses are plotted in Figure 5a and in Figure 5b.

(b) FEAST calculations: A hexagonal mesh with 21 nodes in r direction (6 mm) and 31 nodes in z direction (9 mm) was chosen to model this axisymmetric problem. Because of the set-up in the FEAST code, an integral power of 4.0107, which corresponds to a linear power of 50.4 kW/m, was used. The values of s and q in the analytical solution were selected to ensure that a FEAST predicted temperature profile would be almost identical to that used in the analytical solution (Figure 4b), with the maximum difference between the two being 0.004%. FEAST calculations are compared with analytical solutions in Figure 5a and in Figure 5b. The differences between the FEAST calculated and analytically computed maximum displacement, maximum radial stresses, hoop stresses and axial stresses are within 0.07%, -0.12%, 0.11% and -0.01% respectively.

Case 3-1 (elastic-plastic stresses in a slab subjected to uniaxial tension)

Consider a large slab with a small circular hole in the centre, subjected to uniaxial tension (Figure 6a). If a mesh shown in Figure 6b is used, find the variation of the maximum stress involving elastic-plastic stress with the load.

(a) Tuba's and Stowel's analytical solutions for this problem are available in the open literature[6] for the material of SAE 4130 steel. The stress-strain curve (for SAE 4130 steel) is shown in Figure 7a. In Tuba's and Stowel's analytical solutions, the maximum stress concentration factor $\sigma_{\theta(max)}/\sigma_\infty$ was given with the dimensionless load σ_∞/σ_Y [6]. These curves were digitized first and were then transformed to better defined curves of maximum stress with load (Figure 7b).

(b) FEAST predictions: The mesh consists of 94 nodes and 148 finite elements (see Figure 6b), and its size is 100 mm in both horizontal and vertical directions. The mesh represents one quarter area of the slab shown in Figure 6a. Elastic modulus of 2.068×10^{11} Pa was used for SAE 4130 steel (see Figure 7a). A plastic modulus of 5.856×10^{10} Pa can be found from Figure 7a (the slope of line ab). The FEAST

calculations are compared with Tuba's and Stowel's analytical solutions in Figure 7b. The differences between the FEAST calculations and Tuba's solutions are within -2.42% for the elastic stress and within 1.37% for the plastic stress.

COMPARISON WITH EXPERIMENTAL MEASUREMENTS

Case 4-1 (strain gauge measured strain profiles near the sheath-endcap weld)
Find the strains near the sheath-endcap weld of an experimental fuel element. Compare them with the strain gauge measurement.

(a) Strain gauge measurement of both axial strain profiles and hoop strain profiles near the sheath-endcap weld during compression test (Figure 8a) was conducted in the past. The geometry of the sheath-endcap weld used in the experiment is shown in Figure 8b. Measured strain profiles are shown in Figure 9a and in Figure 9b. The experimental report was not detailed enough to determine the exact location and shape of the upset in the endcap. Despite the uncertainties, this experimental case was included because of the paucity of experimental data.

(b) FEAST predictions: A mesh with 160 nodes and 246 finite elements (Figure 8b) was used for the calculation. Young's modulus of 90 GPa and Poisson's ratio of 0.3 were used. The results of FEAST calculations are compared with the measurements in Figure 9a and in Figure 9b. The FEAST calculations capture all the significant trends exhibited by the measurements. Some minor differences in the absolute values of strain are attributed to the uncertainties in the measurement noted above. Overall, the FEAST calculated strain profiles are quite close to the measurement.

Case 4-2 (two-dimensional photoelastic stress analysis of endcaps)
Find the stress profile in a two-dimensional endcap under an axial load (Figure 10). Compare it with the fringe pattern obtained from a two-dimensional photoelastic stress measurements of endcaps.

(a) In 1972, R.M. Meisel conducted a photoelastic measurement of stress patterns using two-dimensional endcaps made of special transparent plastic material CR-39. Fringes, which indicate the patterns of stress distributions in the endcaps were measured and recorded. In Figure 11, both photo and sketch of fringes are shown for stress patterns under axial loading. Stress concentrations are observed near the weld upset and near some corners.

(b) FEAST predictions: A mesh based on the geometry of the experiment was created. It consists of 276 nodes and 466 finite elements (Figure 12a). Since the fringe pattern obtained from the experiment represents the distribution of the maximum shear stress in the endcap, a plot of contour lines of the maximum shear stress from the FEAST prediction is shown in Figure 12b, for comparison. It can be seen that the FEAST code calculates stress distribution that is remarkably similar to the experimentally observed fringe patterns, with stress concentrations in the vicinity of weld upset and near some of the corners.

DISCUSSION

The overall comparison of FEAST calculations with analytical solutions is summarized in Table 4. There are 18 cases in which direct comparisons of stresses, strains, and displacements can be made. Overall, the FEAST calculations are very close to analytical solutions, for a wide range of conditions involving significant non-linearity, creep, multiaxial stress, and stress concentration. Half the cases

showed a maximum difference of ±1%; the peak difference for all cases was ±5%. No systematic bias were observed (see Table 4).

For the experimental cases, the FEAST calculated strain profiles and iso-stresses are quite close to the experimentally measured profiles (cases 4-1) or to the observed fringe pattern (case 4-2).

APPLICATIONS

In addition to the applications mentioned earlier, the FEAST code has been used recently in the study of multiaxial elastic-plastic stress distributions near the endcap[7], in the end-region design for advanced-cycle fuels that prevent stress-corrosion-cracking (SCC) failure from occurring in that region, in the assessment of residual stresses during long-term storage, and in qualifying fuel for stress-corrosion-fatigue (SCF) during a load following operation[8].

Application of the FEAST code in end-region design: To prevent SCC failure in advanced CANDU fuels, end-region design studies were done in which the effect of the position of the last UO_2 pellet on the stress in the re-entrant corner (notch) was analyzed using the FEAST code. The expansion of the UO_2 pellets during power ramps was believed to be the primary source of stress at the sheath-endcap junction. Hence by moving the position of the last UO_2 pellet away from the junction (re-entrant corner) so that the distance from the junction is greater than the interference-free length, the maximum principal stress in the junction can be lowered to less than that at the ridge, and SCC would not occur in the notch.

Application of the FEAST code in the assessment of residual stresses during long-term storage: To assess fuel integrity under storage conditions, potential fuel degradation processes and their effects on the fuel integrity need to be studied. These potential fuel degradation processes include potential for creep rupture, delayed hydride cracking (DHC) and SCC of the fuel sheath. As a necessary precursor for these studies, the FEAST code was used to provide residual stresses and strains in the fuel sheath at the end of reactor irradiation. The creep and bending effects were taken into account in the calculations. The results can be further used to assess potential fuel degradation processes.

Application of the FEAST code in qualifying fuel for SCF during a load following operation: Analytical assessments were conducted to determine the risk to fuel integrity caused by SCF of the sheath, resulting from expansions and contractions of the pellet during load following operations. The driving force was considered to be the combined influence of SCC caused by the refuelling ramps, plus additional damage caused by corrosion-assisted fatigue (CAF) from the power cycles. The assessments concentrated on conditions at the circumferential ridge of the sheath. The FEAST code was used to account for the effect of sheath bending at the circumferential ridge. For the values of hoop strains that are obtained from the ELESTRES code, the FEAST code provided the values of radial, axial, and shear strains generated by bending near the circumferential ridge. Details of the assessments are described in Reference 8.

Because of the space limitations, only the study of multiaxial elastic-plastic stress distributions near the endcap is briefly described in the present paper.

The endcap of a CANDU fuel element is illustrated in Figure 13. During operation there are 2 sources of tensile stresses that can lead to sheath defects as a result of SCC: the thermal expansion of the pellet, which generally results from power ramps, pushes the sheath and endcap; and the high gas pressure that can be caused by a prolonged operation at high power. Figure 14 shows the loads on an endcap of fuel element and boundary conditions. In the analysis, the ELESTRES code was used first to provide the radial and axial expansions of the fuel pellets, the radial and axial interferences were calculated[7], and

the FEAST code was then used to calculate the detailed axisymmetric multiaxial elastic-plastic stresses in and near the endcap, with the sheath-endcap weld geometry being discretized into 320 to 350 finite elements (200 to 300 nodes).

Typical contours of principal stresses are given in Figure 15. The locations of stress concentrations revealed in this figure are consistent with intuitive expectations. The highest principal stress occurs at the re-entrant corner at the junction of the sheath and the endcap. This location coincides with the location of circumferential cracks observed near the endcaps[7]. The more detailed distribution of stresses are given in Figure 16, which includes radial, hoop, axial, shear, principal and effective stresses. It is seen from this figure that the state of stress at the re-entrant corner is highly multiaxial and that no single component of stress dominates the rest.

From the FEAST results the location of the maximum principal tensile stress was identified at the inner surface. It was hypothesized that the crack might start at this point, and progress perpendicular to the direction of the principal stress. The resulting estimates for the locations and directions of cracks are shown in Figure 17. For all the geometries examined in the study, the FEAST code predicts that the crack is located at the re-entrant corner. This finding is consistent with the observed locations of cracks in Bruce endcaps[7]. The different geometries give different patterns of stresses; hence they result in different predictions for crack directions. Geometries 1 to 4 represent the initial formation and the growth of cracks for 4 combinations of weld upset angles and fillet radii. Geometry 5 contains a weld discontinuity. The code predicts that in geometries 1 to 4 the initial growth of the crack should occur at 40° to 60° from the element axis. This prediction is consistent with the angles of 30° to 60° observed in cracked Bruce fuel[7].

CONCLUSIONS

A detailed validation of the FEAST code was performed for comparison with analytical solutions and experimental observations. The FEAST calculations are in good agreement with the variety of analytical solutions for stresses, strains and displacements. Half the cases showed a maximum difference of ±1%; the peak difference for all cases was ±5%. This agreement shows that the FEAST code correctly incorporates the fundamentals of stress analysis. Further, the calculations of the FEAST code match the variations in axial and hoop strain profiles measured by strain gauges near the sheath-endcap weld during an out-reactor compression test. Moreover, the predicted maximum shear stress distributions in the endcap are consistent with experimental photo-elastic observations. Finally, convergence tests confirmed that the FEAST code converges to the analytical solution, both with mesh refinement and with time-step reduction.

The FEAST code adopted specialized numeric schemes that provide accurate yet fast and stable solutions for the severely non-linear situations normally encountered in the assessment of CANDU fuel. Because of this major strength, the FEAST code has been used in many studies of structural integrity of the CANDU fuel element and bundle and is an important tool for fuel designers and analysts.

ACKNOWLEDGMENTS

The authors gratefully acknowledge D. Rattan for reviewing this manuscript.

NOMENCLATURE

A, B	constant	dt	time step (h)
E	Young's modulus (Pa)	*L*	length (mm)
m, n	constants used in creep calculation	p	pressure (MPa)
q, s	constants used in thermal stress calculation	r	radial distance (mm)
R	radius of cylinder (mm)	t	time (h)
T	temperature (°C)	W	width (mm)

Greek symbols

α	coefficient of thermal expansion (1/°C)	ν	Poisson ratio
σ	normal stress (MPa)	ε	normal strain (%)
δ	displacement (μm)	θ	angular coordinate
Δ	difference (%)		

subscripts

0	initial	c	creep
i	inside	*o*	outside
r	radial	θ	hoop or circumferential
ref	at reference point	Y	at yield point
∞	at infinity		

REFERENCES

1. Tayal, M., "FEAST: A Two-dimensional Non-linear Finite Element Code for Calculating Stresses", 7th Annual Conference of the Canadian Nuclear Society, 1986 June 8-11.

2. Tayal, M., "Modelling CANDU Fuel Under Normal Operating Conditions: ELESTRES Code Description," AECL Report, AECL–9331, 1987.

3 D.N. Fenner, "*Engineering Stress Analysis: A Finite Element Approach with FORTRAN 77 Software*", Ellis Horwood Ltd., New York, NY, 1987.

4 Kraus, H., "*Creep Analysis*", John Wiley & Sons, New York, NY, 1980.

5 Timoshenko, S.P. and Goodier, J.N., "*Theory of Elasticity*", 3rd edition, McGraw-Hill Book Company, New York, NY, 1970.

6 Tuba, I.S., "An Analytical Method for Elastic-Plastic Solutions", Int. J. Solids Structures, Vol. 3, pp. 543-564, 1967.

7 Tayal, M., Hallgrimson, K., Sejnoha, R., Singh, P. and DaSilva, R., "Elastic-Plastic Stress Distributions near the Endcap of a Fuel Element", 4th International Conference on Simulation Methods in Nuclear Engineering, Canadian Nuclear Society, Montreal, Quebec, 1993 June 2-5.

8 Tayal, M., Floyd, M., Rattan, D., Xu, Z., Manzer, A., Lau, J. and Kohn, E., "Load - Following Performance and Assessment of CANDU Fuel", Proceedings of the 6th International Conference on CANDU Fuel, Canadian Nuclear Society, 1999 September 26-29.

Table 1 Validation Matrix: Scenario-to-Phenomenon

Scenario	Phenomenon	
Scenario 1: elastic-plastic stress and strain distributions at sheath-endcap welds	1	elastic stresses and strains in a solid
	2	plastic stresses and strains in a solid
	3	stress concentration
	4	stresses in a solid with endcap geometry
	5	stresses and strains in a solid subjected to distributed loads
	6	stresses and strains in a solid subjected to multiple loads
	7	failure criteria
Scenario 2: elastic-plastic stresses near sheath circumferential ridges during power cycling	1	elastic stresses in a solid
	2	plastic stresses in a solid
	3	thermal stresses in a solid
	4	creep stresses in a solid
	5	stresses in a solid subjected to multiple loads
	6	stresses in a solid subjected to cyclic loads
Scenario 3: elastic-plastic stress distributions in end plates resulting from gravity loads on fuel elements	1	elastic stresses in a solid
	2	plastic stresses in a solid
	3	stress concentration
	4	stresses in a solid subjected to concentrated loads
Scenario 4: sheath creep collapse on pellets under coolant pressure	1	elastic stresses in a solid
	2	plastic stresses in a solid
	3	creep stresses in a solid
	4	stresses in a solid subjected to multiple loads
Scenario 5: hourglassing of UO_2 pellets	1	elastic stresses and strains in a solid
	2	plastic stresses and strains in a solid
	3	thermal stresses and strains in a solid
	4	creep stresses and strains in a solid
	5	stresses and strains in a solid subjected to multiple loads
	6	stresses in a solid with yield strength drop because of temperature rise
Scenario 6: thermal stresses in plenums	1	elastic stresses in a solid
	2	plastic stresses in a solid
	3	thermal stresses in a solid
	4	stresses in a solid subjected to distributed loads
	5	stresses in a solid subjected to multiple loads

Table 2 Validation Matrix: Phenomenon-to-Data Set

	Phenomenon	Data Set
1.	elastic stresses in a solid	case 2-1, case 2-2, case 2-3, case 2-4, case 2-5, case 2-6, case 4-1, case 4-2
2.	plastic stresses in a solid	case 3-1, case 3-2, case 3-3, case 3-4, case 3-5
3.	creep stresses in a solid	case 3-6, case 3-7, case 3-8
4.	thermal stresses in a solid	case 2-7, case 2-8
5.	stresses in a solid subjected to concentrated loads	case 2-3
6.	stresses and strains in a solid subjected to distributed loads	case 2-1, case 2-2, case 2-4, case 2-6, case 3-1, case 3-2, case 4-1, case 4-2
7.	stresses and strains in a solid subjected to multiple loads	case 3-8
8.	stresses and strains in a solid subjected to loading-unloading, and cyclic loads	case 2-5, case 3-4
9.	stresses in a solid with yield strength drop because of temperature rise	case 3-5
10.	failure criteria	case 3-3
11.	stress concentration	case 2-4, case 3-1, case 4-2
12.	stresses in a solid with end cap geometry	case 4-1, case 4-2

Table 3 Feature-based Test Matrix

Feature	Stress, Strain or Displacement Calculation
1) Convergence	case 1-1, case 1-2
2) Elastic stress	case 2-1, case 2-2, case 2-3, case 2-4, case 2-5, case 2-6, case 4-1, case 4-2
3) Plastic stress	case 3-1, case 3-2, case 3-3, case 3-4, case 3-5
4) Creep, stress relaxation	case 3-6, case 3-7, case 3-8
5) Applied concentrated load (e.g., force)	case 2-3
6) Applied distributed load (e.g., pressure)	case 2-1, case 2-2, case 2-4, case 2-6, case 3-1, case 3-2, case 4-1, case 4-2
7) Applied displacement	case 1-2, case 3-6, case 3-7
8) Applied thermal load (thermal stress)	case 2-7, case 2-8
9) Multiple loads	case 3-8
10) Loading-unloading, load cycle	case 2-5, case 3-4
11) Failure criteria	case 3-3
12) Drop of yield strength because of temperature increase	case 3-5

Table 4 Summary of Comparisons FEAST Calculations with Analytical Solutions

Case Number	Difference in σ_{max}, or ε_{max}	Notes	Range
case 1-1	$-0.12\% \le \Delta \le -0.02\%$		±1%
case 1-2	$-0.098\% \le \Delta \le 0\%$		±1%
case 2-1	$0.83\% \le \Delta \le 3.46\%$	difference in $\delta_{max} \le 3.85\%$	±4%
case 2-2	$-1.53\% \le \Delta \le 0\%$	difference in $\delta_{max} \le 1.76\%$	±2%
case 2-3	$0\% \le \Delta \le 1.22\%$		±2%
case 2-4	$0\% \le \Delta \le 2.53\%$		±3%
case 2-5	$-0.27\% \le \Delta \le -0.04\%$	difference in $\delta_{max} \le 0.30\%$	±1%
case 2-6	$-0.42\% \le \Delta \le -0.03\%$		±1%
case 2-7	$-1.94\% \le \Delta \le 2.52\%$		±3%
case 2-8	$-0.12\% \le \Delta \le 0.11\%$	difference in $\delta_{max} \le 0.07\%$	±1%
case 3-1	$-2.12\% \le \Delta \le 1.37\%$		±3%
case 3-2	$-4.32\% \le \Delta \le 3.95\%$		±5%
case 3-3	$-0.09\% \le \Delta \le 0\%$		±1%
case 3-4	$-0.75\% \le \Delta \le 0.13\%$		±1%
case 3-5	$-0.02\% \le \Delta \le 0.04\%$		±1%
case 3-6	$-2.23\% \le \Delta \le 0.1\%$		±3%
case 3-7	$-1.38\% \le \Delta \le 0\%$		±2%
case 3-8	$-0.12\% \le \Delta \le 0.34\%$		±1%

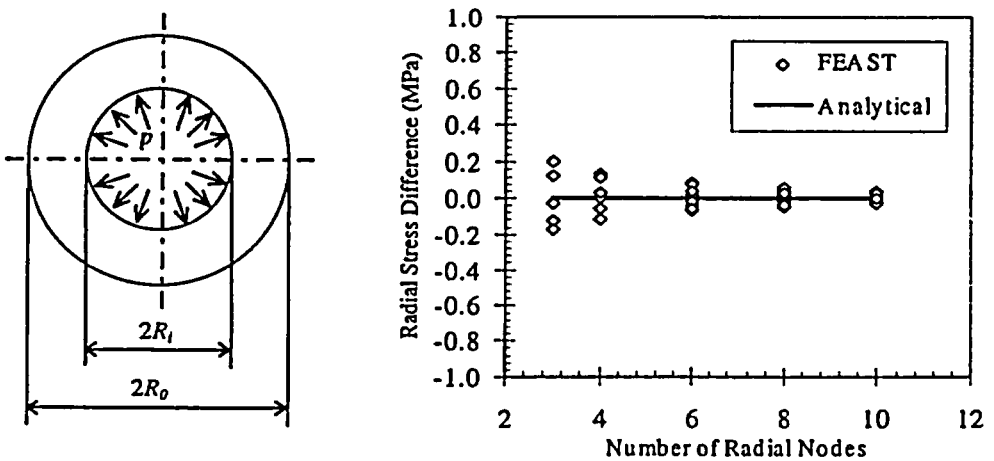

Figure 1 Mesh Convergence of the FEAST Code (case 1-1): (a) A Long Hollow Cylinder, (b) Mesh Convergence

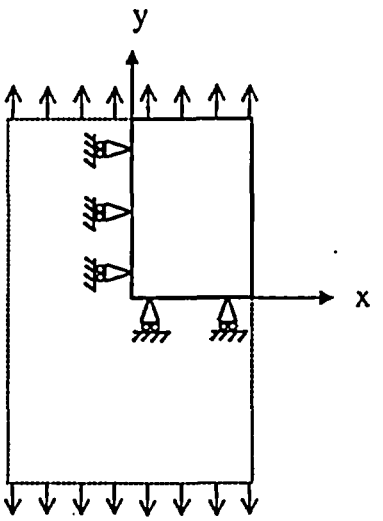

Figure 2 Stress Relaxation during Creep (Case 1-2)

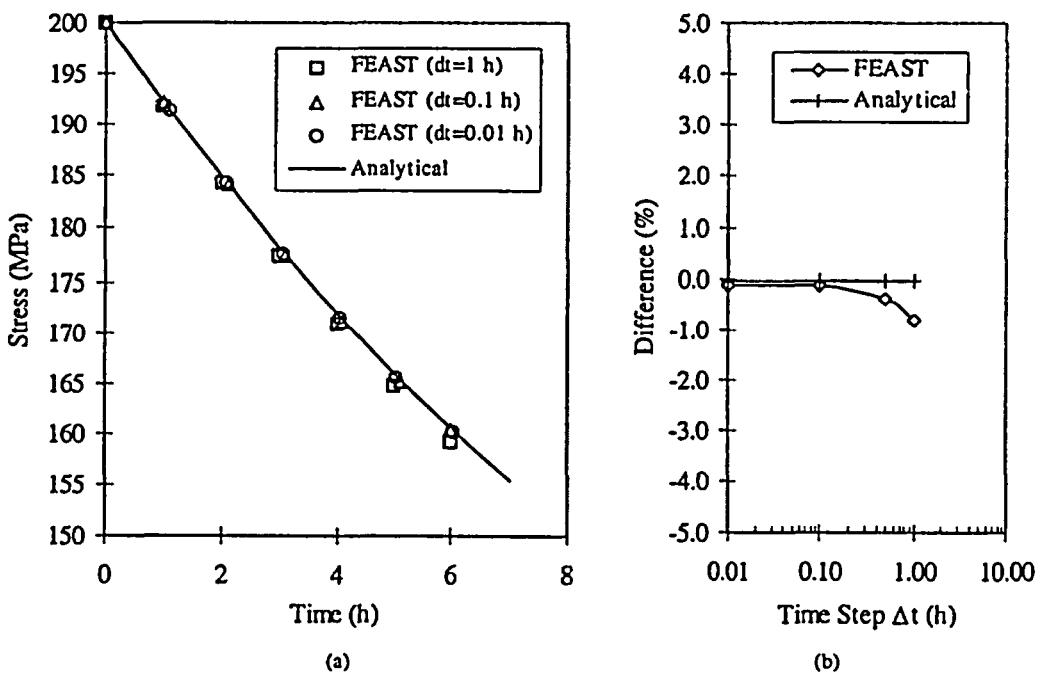

Figure 3 Time Step Convergence of FEAST (Case 1-2): (a) Effect of Time Step, (b) Convergence with Time-step Reduction

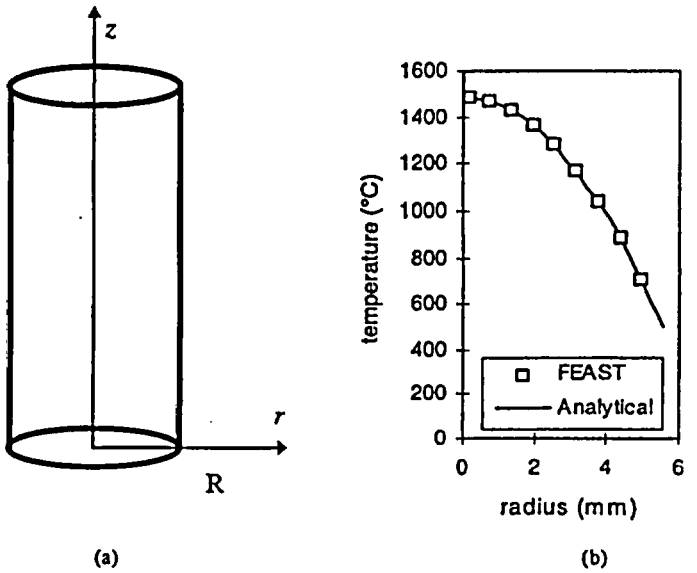

Figure 4 Long Solid Cylinder with Parabolic Temperature Distribution (Case 2-8): (a) Long Solid Cylinder, (b) Parabolic Temperature Distribution

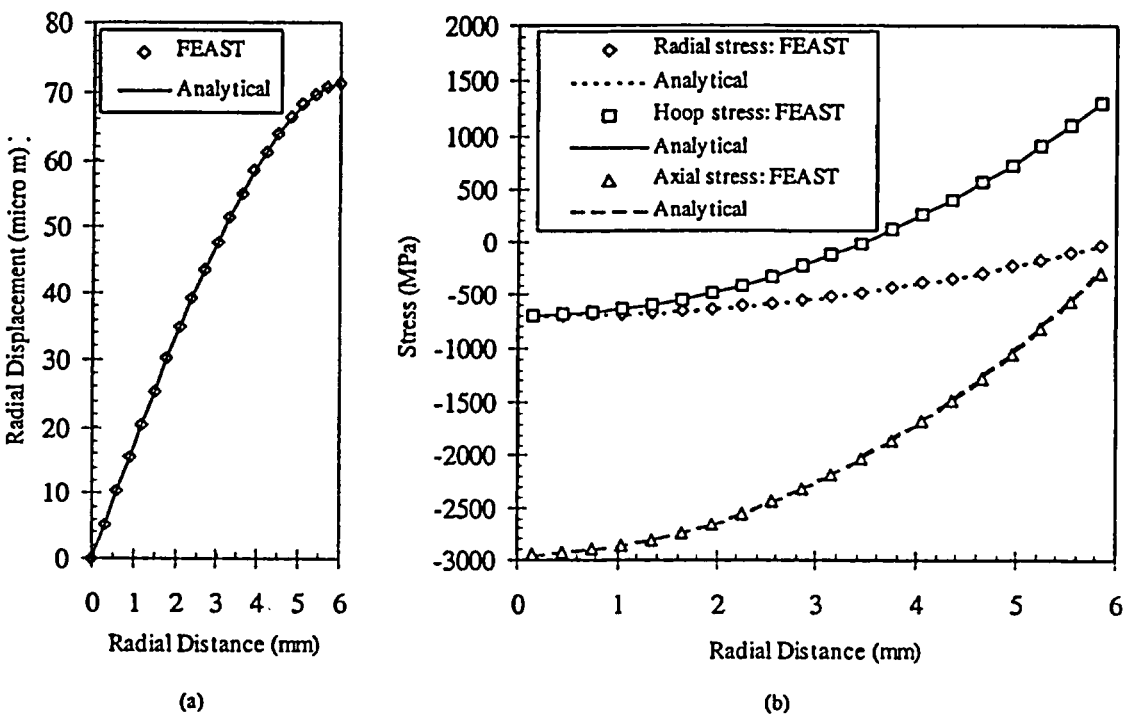

Figure 5 Displacement and Thermal Stresses in the Solid Cylinder (Case 2-8): (a) Radial Displacement, (b) Thermal Stresses

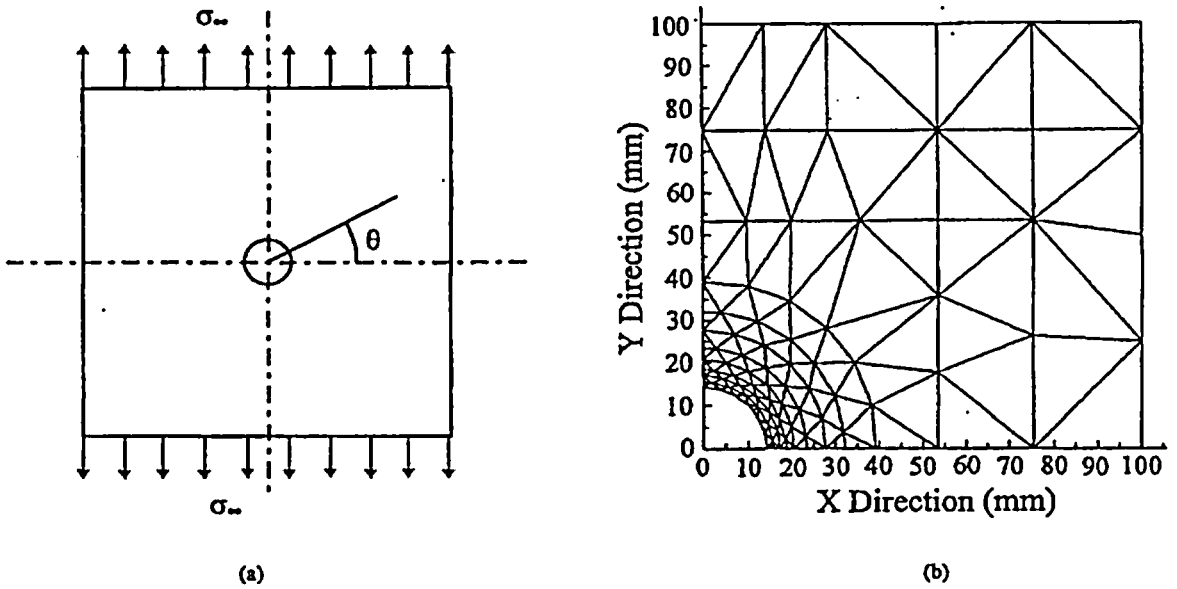

Figure 6 Elastic-Plastic Loading on a Slab with a Small Hole (Case 3-1): (a) Slab, (b) Mesh Used in FEAST Calculation

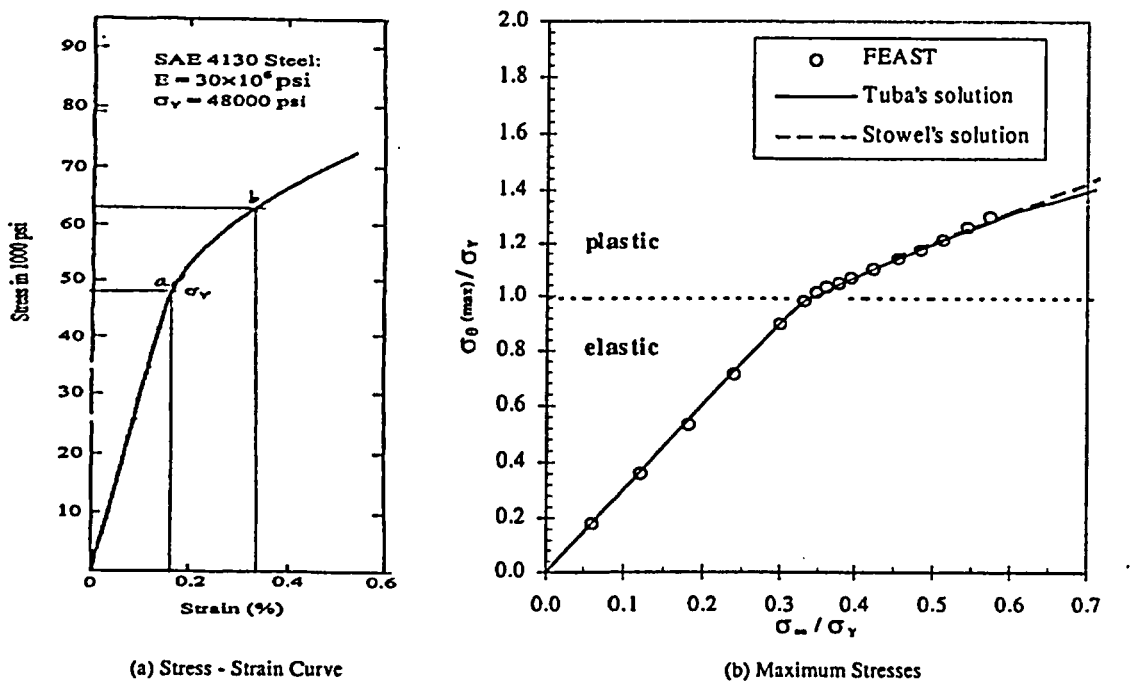

Figure 7 Maximum Stress near a Hole in a Large Slab (Case 3-1)

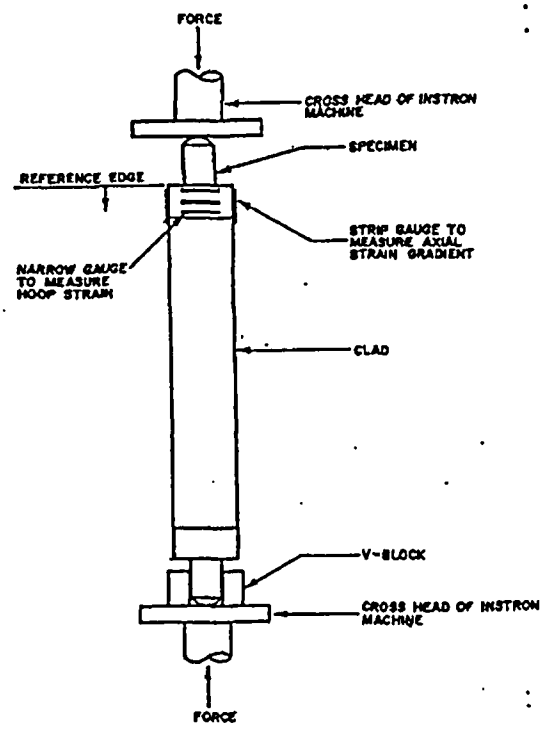

(a) Compression Test

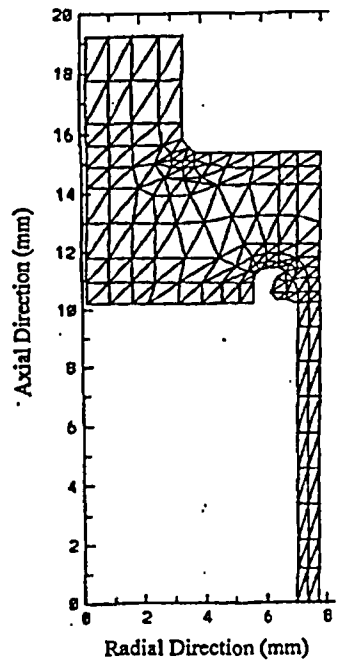

(b) Mesh of Sheath-Endcap Weld

Figure 8 Strain Measurement near Sheath-Endcap Weld (Case 4-1)

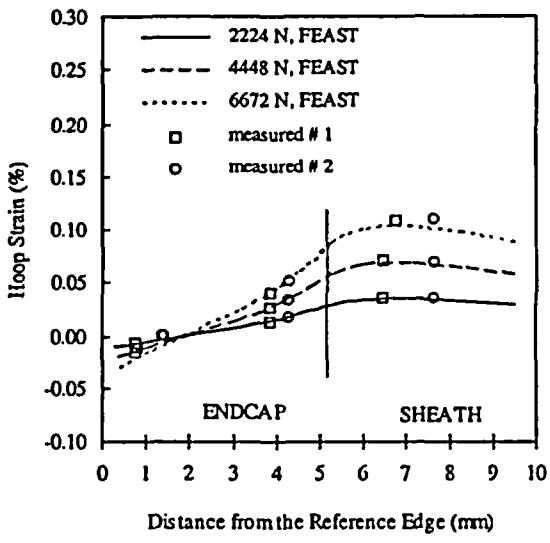

(a)

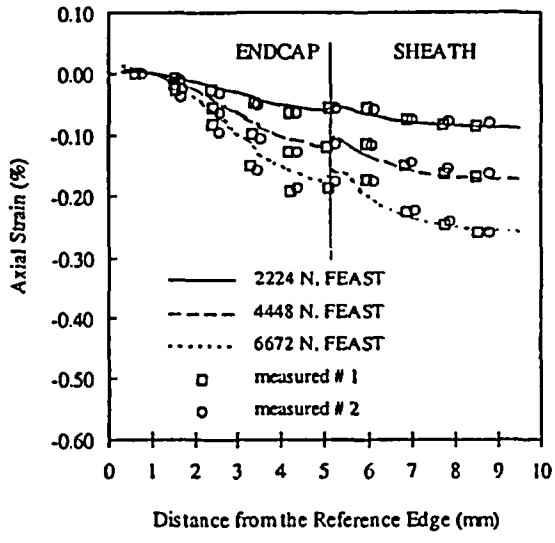

(b)

Figure 9 Measured and Calculated Strains around the Sheath-Endcap Weld (Case 4-1) (a) Hoop Strains, (b) Axial Strains.

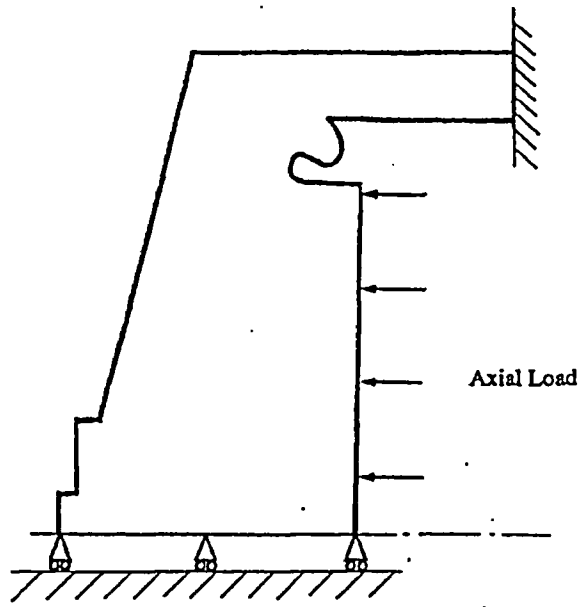

Figure 10 Endcap under Axial Load (Case 4-2)

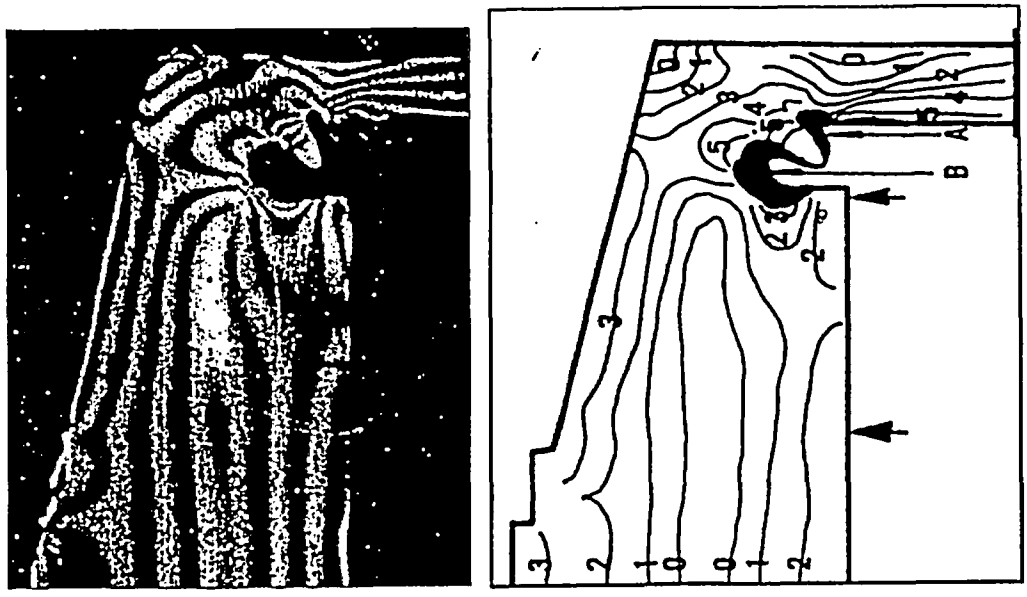

(a) photo (b) sketch

Figure 11 Fringe Pattern from Two-dimensional Photoelastic Experiment (Case 4-2)

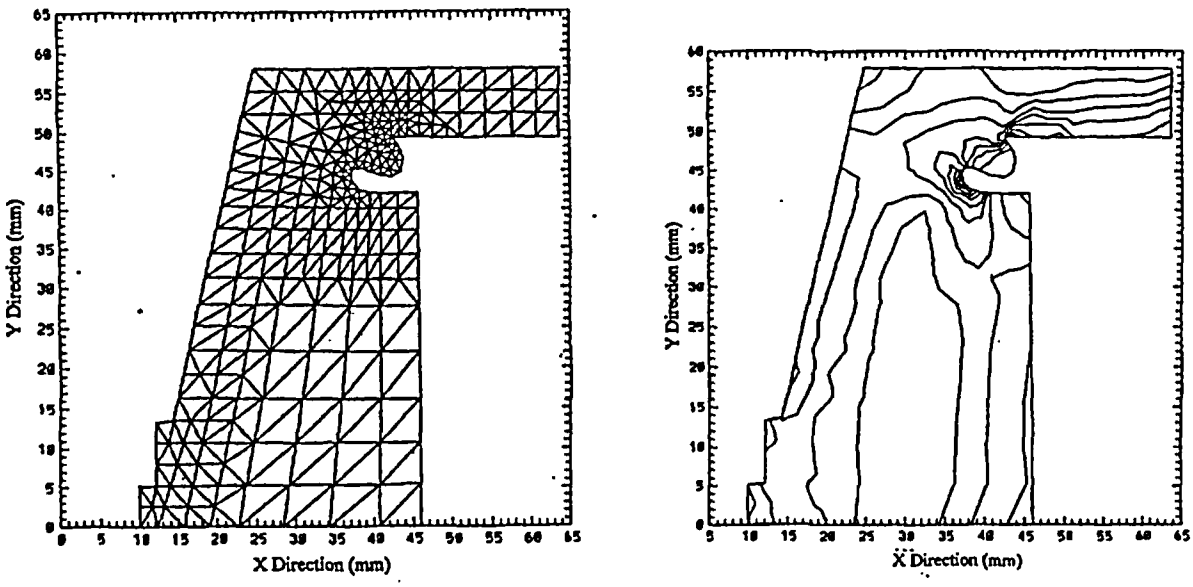

(a) (b)

Figure 12 FEAST Prediction of Stress Contour Lines in the Endcap (Case 4-2): (a) Mesh Used, (b) Stress Contour Lines in the Endcap

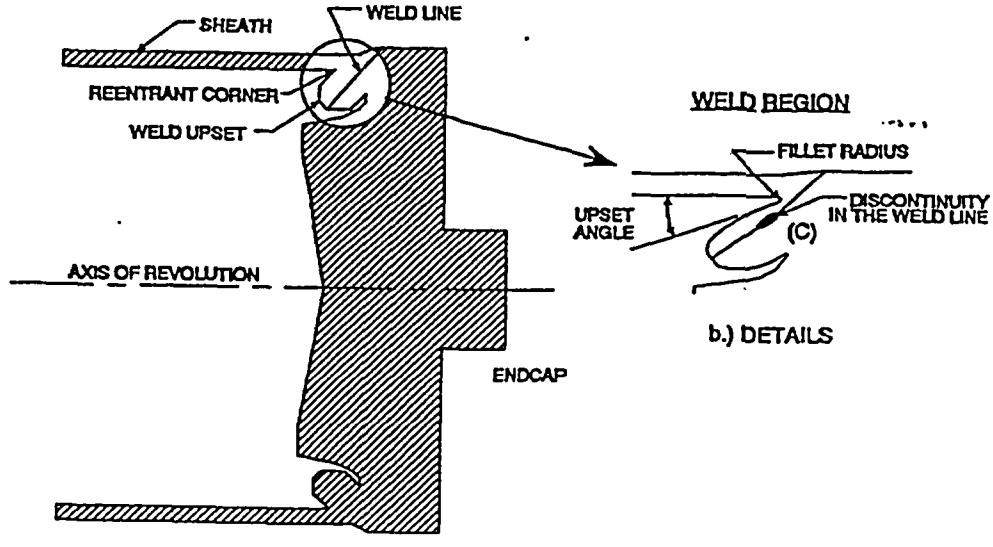

(a) OVERVIEW

Figure 13 Endcap of a CANDU Fuel Element

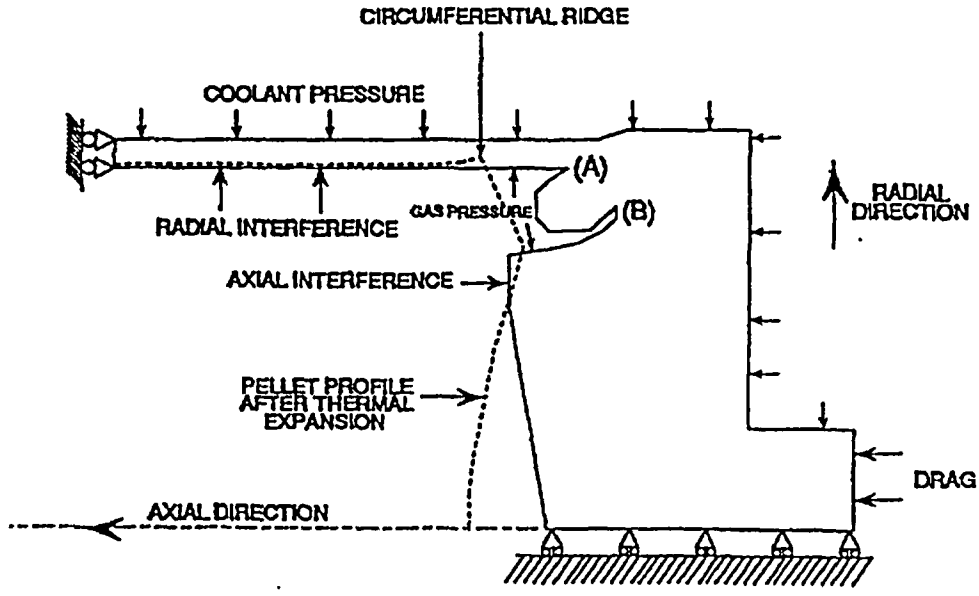

Figure 14 Endcap: Loads and Boundary Conditions

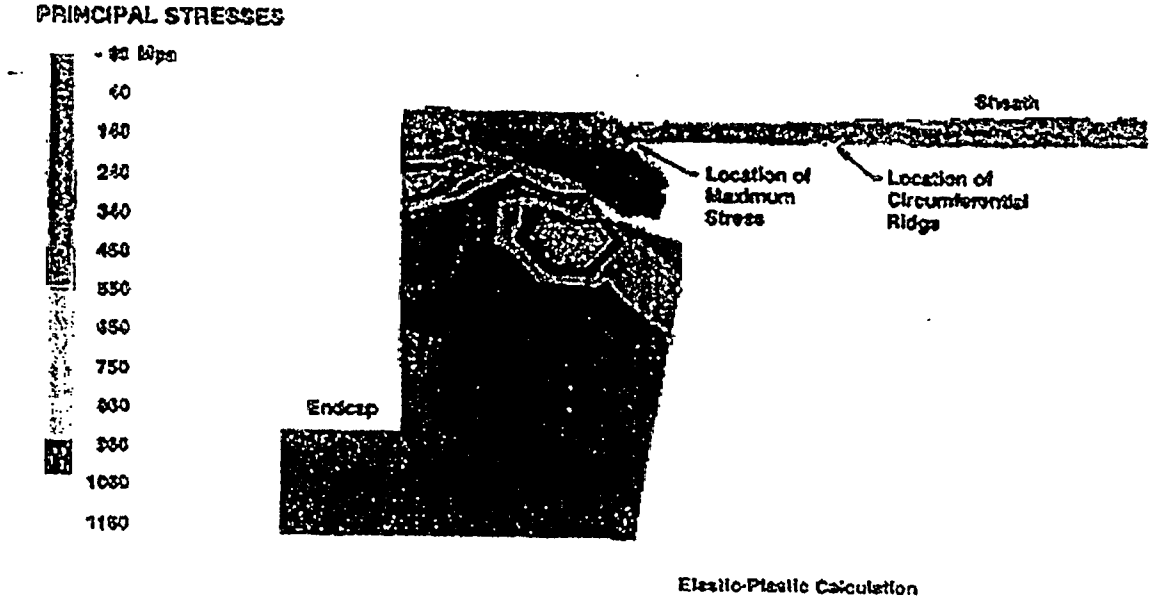

Figure 15 FEAST Predicted Principal Stresses near and in an Endcap

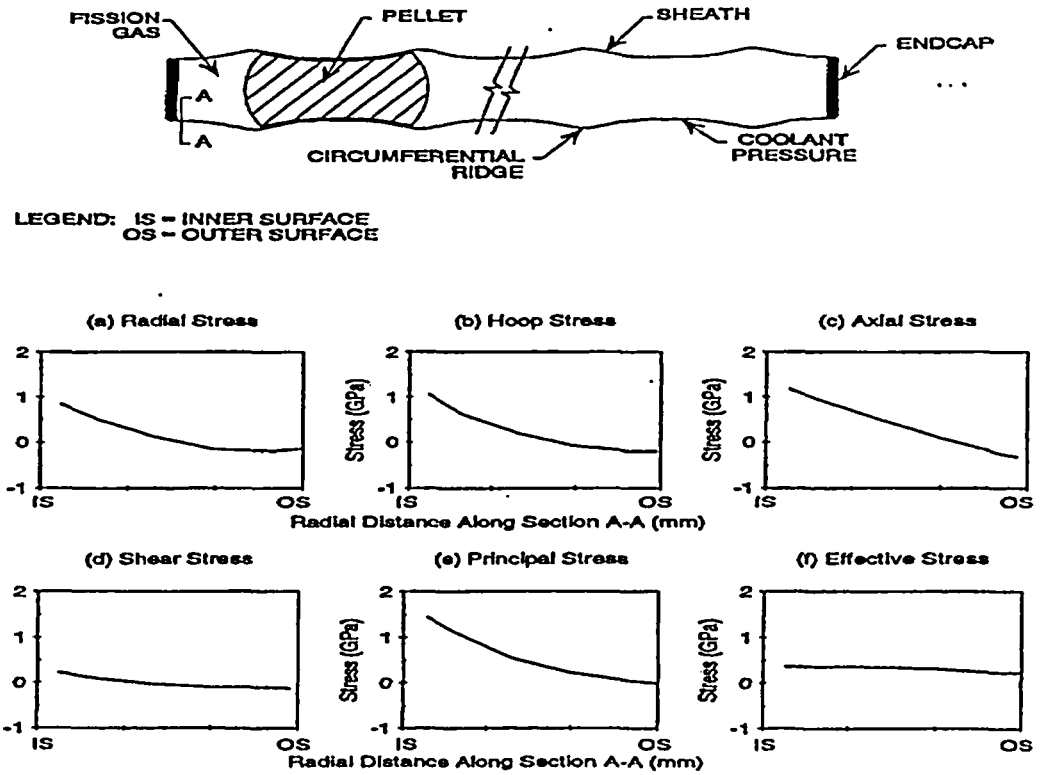

Figure 16 Predicted Elastic-Plastic Stresses in Sheath at the Re-entrant Corner

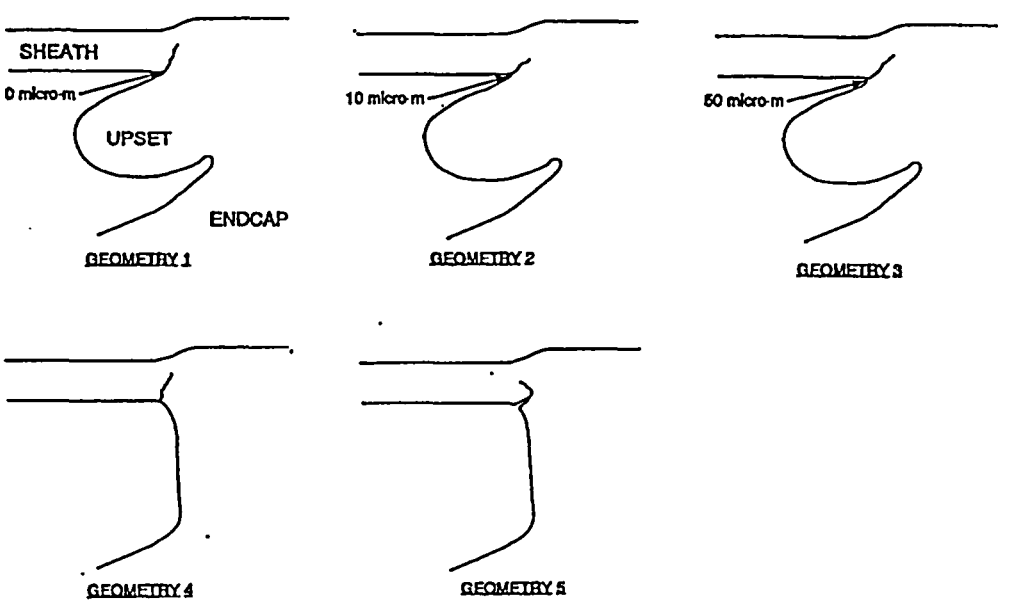

Figure 17 Predicted Locations and Directions of Cracks